Biosensors and Bioelectrics 225 (2023) 115060

Contents lists available at ScienceDirect

Biosensors and Bioelectronics

journal homepage: www.elsevier.com/locate/bios

Ultra-soft and highly stretchable tissue-adhesive hydrogel based multifunctional implantable sensor for monitoring of overactive bladder

Byungkook Oh [a,1], Young-Soo Lim [b,1], Kun Woo Ko [a], Hyeonyeob Seo [c], Dong Jun Kim [d], Dukyoo Kong [e], Jae Min You [e], Hansoul Kim [e], Taek-Soo Kim [d], Seongjun Park [c,f], Dong-Soo Kwon [e], Joon Chae Na [j], Woong Kyu Han [k], Sung-Min Park [b,g,h,i,**], Steve Park [a,f,*]

[a] Department of Materials Science and Engineering, Korea Advanced Institute of Science and Technology (KAIST), 291 Daehak-ro, Yuseong-gu, Daejeon, Republic of Korea
[b] Department of Convergence IT Engineering (CiTE), Pohang University of Science and Technology (POSTECH), 77 Cheongam-ro, Nam-gu, Pohang-si, Gyeongsangbuk-do, Republic of Korea
[c] Department of Bio and Brain Engineering, Korea Advanced Institute of Science and Technology (KAIST), 291 Daehak-ro, Yuseong-gu, Daejeon, Republic of Korea
[d] Department of Mechanical Engineering, Korea Advanced Institute of Science and Technology (KAIST), 291 Daehak-ro, Yuseong-gu, Daejeon, Republic of Korea
[e] Roen Surgical Inc, 193, Munji-ro, Yuseong-gu, Daejeon, 34051, Republic of Korea
[f] KAIST Institute for Health Science and Technology, 291 Daehak-ro, Yuseong-gu, Daejeon, Republic of Korea
[g] Department of Electrical Engineering, Pohang University of Science and Technology (POSTECH), 77 Cheongam-ro, Nam-gu, Pohang-si, Gyeongsangbuk-do, Republic of Korea
[h] Department of Mechanical Engineering, Pohang University of Science and Technology (POSTECH), 77 Cheongam-ro, Nam-gu, Pohang-si, Gyeongsangbuk-do, Republic of Korea
[i] Institute of Convergence Science, Yonsei University, Seoul, Republic of Korea
[j] Department of Urology, Urological Science Institute, Yonsei University College of Medicine, Seoul, Republic of Korea
[k] Department of Urology, Urological Science Institute, Yonsei University College of Medicine, Center of Uro-Oncology, Yonsei Cancer Hospital, Seoul, Republic of Korea

ARTICLE INFO

Keywords:
Hydrogels
Strain sensors
EMG sensors
Soft-Rigid hybrid structures
In-vivo measuring of overactive bladder models of rat

ABSTRACT

A highly stretchable and tissue-adhesive multifunctional sensor based on structurally engineered islets embedded in ultra-soft hydrogel is reported for monitoring of bladder activity in overactive bladder (OAB) induced rat and anesthetized pig. The use of hydrogel yielded a much lower sensor modulus (1 kPa) compared to that of the bladder (300 kPa), while the strong adhesiveness of the hydrogel (adhesive strength: 260.86 N/m) allowed firm attachment onto the bladder. The change in resistance of printed liquid metal particle thin-film lines under strain were used to detect bladder inflation and deflation; due to the high stretchability and reliability of the lines, surface strains of 200% could be measured repeatedly. Au electrodes coated with Platinum black were used to detect electromyography (EMG). These electrodes were placed on structurally engineered rigid islets so that no interfacial fracture occurs under high strains associated with bladder expansion. On the OAB induced rat, stronger signals (change in resistance and EMG root-mean-square) were detected near intra-bladder pressure maxima, thus showing correlation to bladder activity. Moreover, using robot-assisted laparoscopic surgery, the sensor was placed onto the bladder of an anesthetized pig. Under voiding and filling, bladder strain and EMG were once again monitored. These results confirm that our proposed sensor is a highly feasible, clinically relevant implantable device for continuous monitoring OAB for diagnosis and treatment.

* Corresponding author. Department of Materials Science and Engineering, Korea Advanced Institute of Science and Technology (KAIST), 291 Daehak-ro, Yuseong-gu, Daejeon, Republic of Korea.
** Corresponding author. Department of Convergence IT Engineering (CiTE), Pohang University of Science and Technology (POSTECH), 77 Cheongam-ro, Nam-gu, Pohang-si, Gyeongsangbuk-do, Republic of Korea.
E-mail addresses: sungminpark@postech.ac.kr (S.-M. Park), stevepark@kaist.ac.kr (S. Park).
[1] Equal Contribution.

https://doi.org/10.1016/j.bios.2023.115060
Received 5 October 2022; Received in revised form 2 January 2023; Accepted 3 January 2023
Available online 4 January 2023

1. Introduction

Overactive bladder (OAB) is a collective term for a group of urinary symptoms characterized by frequent and sudden urge to urinate due to detrusor overactivity, which leads to uncontrolled micturition reflex (Steers, 2002). While prevalence estimates vary among studies, over 20% of people over the age of 40 suffer from OAB according to Nurses' Health study (Nagai et al., 2021). OAB may cause extreme discomfort to the patient, preventing them from partaking in normal everyday activities, consequently causing various psychological problems such as anxiety and depression (Lai et al., 2016). Furthermore, long-term neglect of OAB can lead to severe chronic conditions such as kidney failure and renal malfunction (Fowler et al., 2008; Herbison and Arnold, 2009; Scarneciu et al., 2021).

Despite the high prevalence of OAB, its treatment still mainly relies on prescribed medications, which has shown to be ineffective in patients with severe OAB (Millard and Halaska, 2006). Thus, device based neuromodulation modalities such as tibial or sacral nerve stimulation have been proposed since 1983 and was approved for treatment in 1997 (Lee et al., 2021). For these procedures, nerves directly or indirectly connected to the bladder are electrically stimulated to reduce the overactivity of the bladder. One potential issue with these treatments is that nerves are being stimulated without the monitoring of bladder activity, which can potentially cause side-effects due to excessive stimulation or render the treatment ineffective (Banakhar et al., 2012). To overcome the limitations of such continuous, open-loop stimulation, there have been extensive efforts in developing selective or closed loop neuro-stimulation modalities, but these efforts have not been successful for bladder control due to a lack of efficient bladder activity monitoring method (Ju et al., 2022; Lo and Widge, 2017; Mirza et al., 2019). Therefore, real-time monitoring of bladder activity would be highly beneficial, as it can be used as a feedback for the neurostimulators so that nerve stimulation can be automatically tuned based on bladder activity. With this feedback control, neuromodulation for fully-automated personalized treatment becomes possible.

Various bladder activity monitoring devices have been previously reported (Arab Hassani et al., 2020; Jang et al., 2020). These devices have been fabricated with silicone-based elastomers as substrates, which have Young's modulus (will be referred to as modulus herein) in the range of the MPa to the GPa (Arab Hassani et al., 2020; Jang et al., 2020.; Roche, 2019), far larger than that of human bladder (~300 kPa) (Li et al., 2014). Large mechanical mismatch can cause physical damage (Chen et al., 2018; Kim et al., 2017) to the contacting bladder tissue resulting in significant inflammation and obstruction of normal bladder motion. With this drawback, sensors with significant mechanical mismatch are not suitable for implantable sensors that need long-term operation (Lacour et al., 2016; Someya et al., 2016; Wellman et al., 2018; Yuk et al., 2019, 2022). In addition, the operation of some of these devices were demonstrated by completely wrapping or surrounding the device around mouse bladder (Arab Hassani et al., 2020; Jang et al., 2020), rather than them being adhered onto the surface of the bladder tissue. However, this approach makes the surgical procedure extremely difficult or impossible for human implantation. Hence, a low modulus ultra-soft sensor than can be adhered seamlessly to the surface of the bladder is preferred for clinical translation.

Past works have focused on sensing the mechanical contraction and relaxation to monitor the status of the bladder. The bladder activity is directly controlled by mechanical movement of the detrusor muscle located in the wall of the bladder; however, the signal quality of the mechanical movement of the bladder can be largely affected by the body motion during daily life. Since the mechanical motion of the bladder is preceded by the reception of electrical signals from the nerves, electromyography (EMG) signal is also expected to be present during bladder movement and serve as an additional digital phenotype for OAB. Thus, simultaneously measuring EMG and expansion/contraction of the bladder would not only accurately keep track of bladder mechanical (physical) state, but also indirectly monitor the neurological state for micturition reflex. In this regard, Jang et al. fabricated underactive bladder sensor measuring both strain and EMG (Jang et al., 2020). However, the quantitative analysis for the EMG signals as a digital probe for OAB has not been presented in this study. Therefore, to understand the abnormal EMG signals associated with the OAB, the EMG analysis using the disease model still needs to be performed.

Here, we report multifunctional bladder activity sensor based on *u*ltra-*s*oft *h*ydrogel combined with *s*tructurally-engineered *i*slets (USH–SI sensor), which can overcome the limitations of previously reported bladder sensors. Since detrusor muscle is controlled by the neural activity, we hypothesized that the full electromechanical measurement is required for accurately monitoring overactive bladder symptoms. In this perspective, we designed our USH-SI sensor that can monitor both mechanical (strain sensor to measure contraction/relaxation) and bioelectrical (EMG sensor to measure neural signal causing detrusor muscle contraction) activities of the bladder in one platform. With the proposed design, the USH-SI sensor is capable of measuring in-vivo strain and EMG signals of the bladder, thus allowing simultaneous monitoring of detrusor muscle locomotion and neural activity for more comprehensive and accurate micturition detection. Although the OAB mechanism has not been fully discovered, it is well known that the cause of the OAB can be myopathic and neuropathic (MENG et al., 2012). Such various causes of OAB increases complexity for interpretation of bladder activity and OAB symptom. The necessity of combining two measurements together need to be explicitly addressed for mutual validation and precise analysis.

The use of hydrogel as the substrate material yields low modulus of ~1 kPa, far lower than the modulus of human bladder. Furthermore, the high-water content (similar to that of human tissues) and surface functional groups of hydrogels form a strongly adhered and natural seamless interface with the bladder tissue (Seiffert and Oppermann, 2007). The adhesion of the hydrogel substrate to the surface of the bladder makes it unnecessary to design a large device to cover or surround the entire bladder. Therefore, the proposed technology can also contribute to sensor miniaturization that can enable laparoscopic surgical implantation, which can potentially minimizes recovery time and complications to the patients (Hwang et al., 2014; Maeso et al., 2010). Thus, the feasibility of laparoscopic implantation was demonstrated on a pig in this study. The strain sensor was made with liquid metal particle-based thin-films printed directly on the hydrogel substrate, which due to its ultra-high stretchability and durability, allowed bladder movement that yields strains of up to 300% to be measured. The EMG sensors were made by coating Platinum black (PtB) on Au electrodes, which showed relatively low impedance of 15 Ω at 1 kHz and consequently higher signal-to-noise ratio (SNR: 22.84 dB) compared to that of the reference PtB-uncoated Au electrodes (120 Ω at 1 kHz and SNR of 14.42 dB). The EMG sensors were placed on structurally engineered rigid polyimide (PI) islets to ensure stable operation under high strains. Using the USH-SI sensors, bladder activity in OAB induced rats and an anesthetized pig were measured and analyzed. The experimental results clearly showed that resistance change of the strain sensor accurately represented bladder volume change, and more prominent activation of EMG signals could be found at urination points. Results from OAB induced rats showed correlation coefficient (r) of −0.8105 between IBP (intra-bladder pressure) and strain sensor resistance, and 1.81 times higher EMG RMS (root-mean-square) near IBP peaks, indicating that the proposed device can accurately detect the urination time points. These results together confirm the feasibility of our sensor design for accurate in-vivo measurement of bladder activity that is potentially safe and relatively easy to surgically implant. We project that our USH-SI sensor can be combined with neurostimulators in the future to enable feedback-based neural stimulation system, thus providing a pathway for more effective treatment of OAB.

2. Results and discussion

USH-SI sensor simultaneously measures bladder volume state and detrusor muscle activity using strain and EMG sensors, respectively (Fig. 1A). For strain, peaks in the resistance indicated maximum contraction of the bladder. For EMG, RMS of the EMG signal (EMG RMS) was calculated to determine the time at which EMG activation had increased. These points in a time series were validated from both signals and considered to be the time at which urination occurred, and thus the interval between these urination points can be utilized as a criterion for diagnosing OAB.

For this study, polyacrylamide (PAAm) hydrogel was used as the substrate. One critical issue with PAAm (and with hydrogels in general) as implantable substrates, however, is their eventual swelling and change in electrical properties due to the gradual absorption of biofluids in the body (Lee et al., 2018; Zhang et al., 2018). To address this issue, we have developed an anti-swelling coating technique (see Materials and Methods in Supporting information for coating procedure) that can prevent absorption of water and biofluids in the body. This technique is applicable to various hydrogels that have low sol-gel transition temperatures, while imposing negligible changes in mechanical properties and surface properties to the hydrogels. Further discussion of this technique will be reported in a future work. To test the effect of our anti-swelling coating, we have immersed two substrates (with and without the anti-swelling coating) in phosphate buffer solution (PBS) for 30 days. Once a day, the relative change in the weight of the substrates (g_f/g_o, where g_f and g_o are the weight of the substrate at a given day and initially, respectively) were measured. As depicted in Fig. 1B, without the anti-swelling coating, the weight increased by ~4 times after a week. On the contrary, the substrate with the anti-swelling coating had a negligible change in the weight (~1.2 times) over the 30 day period, thus proving their relative long-term stability (see Fig. S1 for electrical characteristics comparison). Fig. 1C is the stress versus strain curve of the PAAm substrate with and without the anti-swelling coating. As depicted in Fig. S2, the Young's Modulus of the hydrogel substrate slightly increased from 0.8 to 1 kPa after coating. Thus, even after the anti-swelling coating, Young's modulus of the substrate is still much lower than that of bladder (~300 kPa) (Chitrakar et al., 2022; Li et al., 2014), making our substrate feasible for bladder attachment, likely with minimal effect on the natural motion of the bladder.

Fig. 1D are the peel tests of various samples on pig bladder tissue in air environment. For film attachment of PAAm substrate on bladder tissue, a hydrogel-based adhesive (detailed in Materials and Methods in Supporting information) was utilized. The results show that an adhesive strength of 260.86 N/m is needed to peel off the PAAm substrate; whereas, 2.15 N/m is needed to peel off the silicone-based substrates previously used. This difference can be attributed to the strong binding of the adhesive to both the bladder tissue and to the PAAm substrate by

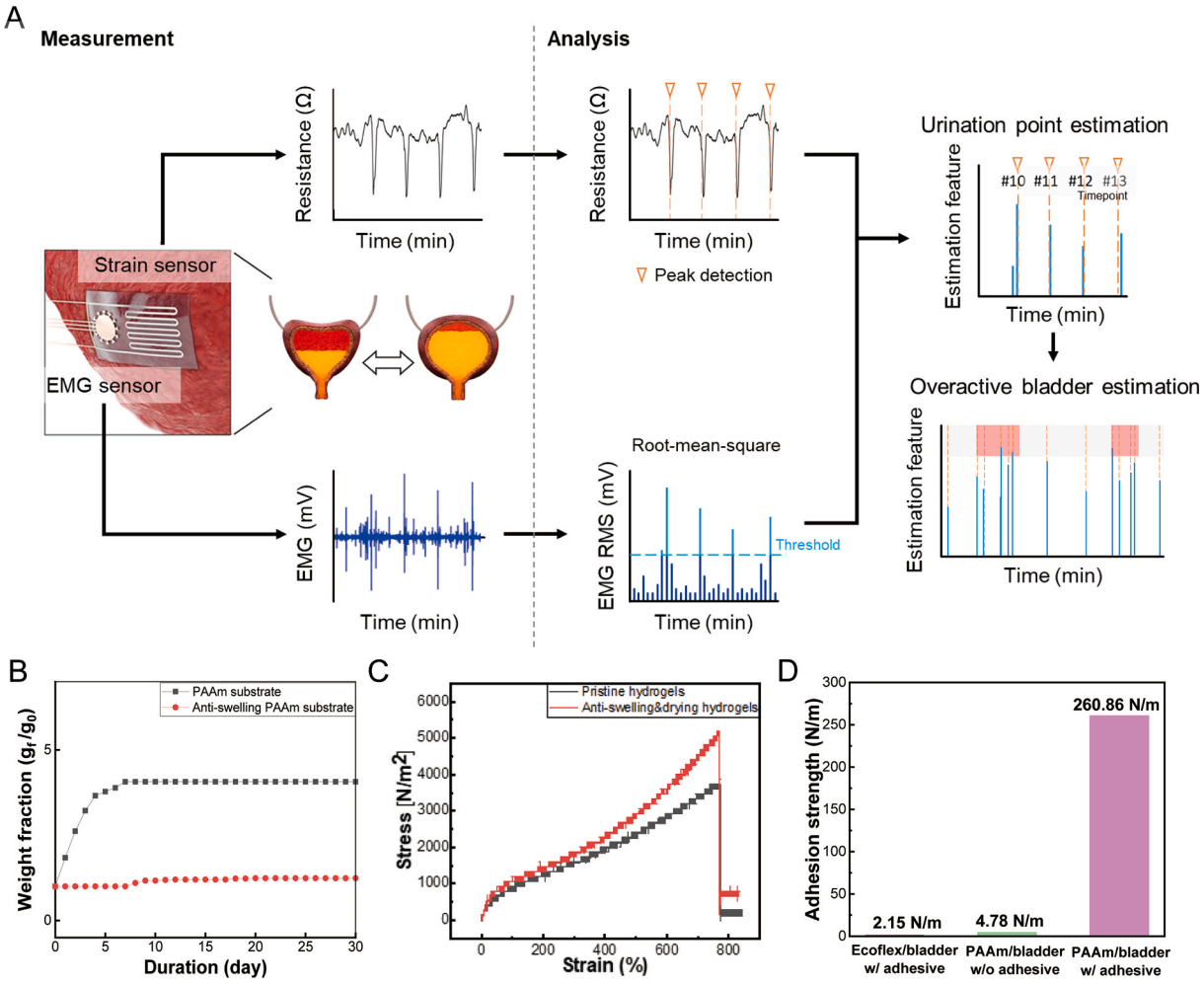

Fig. 1. (A) The schematic illustration for in-situ diagnosis process of overactive bladder rat model; (B) Plot of soaking duration versus relative change of PAAm w/ and w/o anti-swelling coating in PBS solution; (C) The strain-stress curve of pristine PAAm and anti-swelling PAAm; (D) The plot of adhesion strength between conventional silicone rubber (Ecoflex-0020) and anti-swelling PAAm substrates w/and w/o hydrogel-based adhesive. The PAAm substrate had significantly higher adhesion strength (260 N/m) than conventional silicone rubber substrate (2.15 N/m).

anchored amine group and Calcium ions (Seiffert and Oppermann, 2007; Seo et al., 2018). Fig. S3 shows details of the adhesion test. Additionally, we conducted the peel tests of the same samples on pig bladder tissue in harsh wet environment, containing phosphate buffer solution (PBS) as shown in Fig. S4. The results show that an adhesive strength of 66.96 N/m is needed to peel off PAAm substrate, whereas, 1.93 N/m is needed to peel off the silicone-based substrates.

On the PAAm substrate, a strain sensor and EMG sensor were integrated, as detailed in Materials and Methods in Supporting information and in Fig. S5. Since bladder stretches to a maximum of ~300% (Jang et al., 2020; Shimoni et al., 2015) (typically <200% for OAB patients) (Redmond et al., 2019), a highly stretchable and mechanically durable material was needed for strain sensing. In this regard, eutectic gallium-indium alloy-based particles (EGaIn*) were used (Lee et al., 2022) due to its high softness, stretchability, biocompatibility (Chiew et al., 2021; Kim et al., 2018). Furthermore, EGaIn* can be directly printed on PAAm as depicted in Fig. 2A and B. Here, meniscus-guided coating was utilized, where the nozzle is dragged across a heated PAAm substrate (60 °C) at a speed of 6.4 mm/s. This process deposits EGaIn* lines (linewidth of 220 μm) with an initial resistivity of 1.17 Ωmm. Fig. 2C is a top view scanning electron microscopy (SEM) image of the printed EGain* film, where closely packed EGain* are observed.

The feasibility of the EGaIn*-based strain sensor printed on PAAm was investigated, firstly by measuring the resistance under lateral strain. The strain sensor was observed to have the low hysteresis (less than 5%) and stable operation up to 300% strain (Fig. S6) with the gauge factor of 1.1. Next, the strain sensor was attached on a balloon-based artificial bladder; the initial and expanded state of the balloon with the attached strain sensor is shown in Fig. 2D. Fig. 2E depicts relative resistance change under 10,000 micturition cycles at 200% strain, which demonstrates long-term durability and reliability of the strain sensor. Fig. 2F is the relative resistance change at various strains, confirming that different strain values can be measured.

For EMG sensing, it is critical to lower the electrode impedance so that electrical signal can be reliably measured with minimal noise. In this regard, we have utilized gold electrode coated with Pt black (PtB) (Abbott et al., 2020). PtB coating on the surface of Au electrodes increases the surface area of electrodes which results in an increase in capacitance of electrodes and as the result, the electrode impedance is lowered. Fig. 2G shows the EMG sensor (fabricated on 50 μm thick PI islets) placed on the PAAm substrate. The electrical leads of the EMG sensor were connected to external wiring (PI film with patterned Ti/Au (5 nm/100 nm) electrodes) using anisotropic conductive film (ACF) (Hwang et al., 2021), composed of gold nanoparticles embedded within polystyrene-block-poly (ethylene-ran-butylene)-block-polystyren-graft-maleic anhydride (SEBE-g-MA), as seen in Fig. S7. Fig. 2H is the impedance versus frequency plot, showing that with the PtB coating, the impedance decreases significantly over a large frequency range. As seen in the inset, at 1 kHz, the impedance for the gold electrode without and with PtB coating were 121 Ω and 15 Ω, respectively. Fig. S8 shows optical and SEM images of PtB coated on Au.

Since the PAAm substrate stretches to several hundred percent in strain repetitively during the micturition cycles, PI islet placed on the PAAm substrate can easily delaminate due to the large mechanical mismatch between the two materials (Yuk et al., 2019; Pei et al., 2021; Bovone et al., 2021). To address this issue, we have structurally engineered the islets into the shape of Ferris-wheels (FWIs) (inner and outer

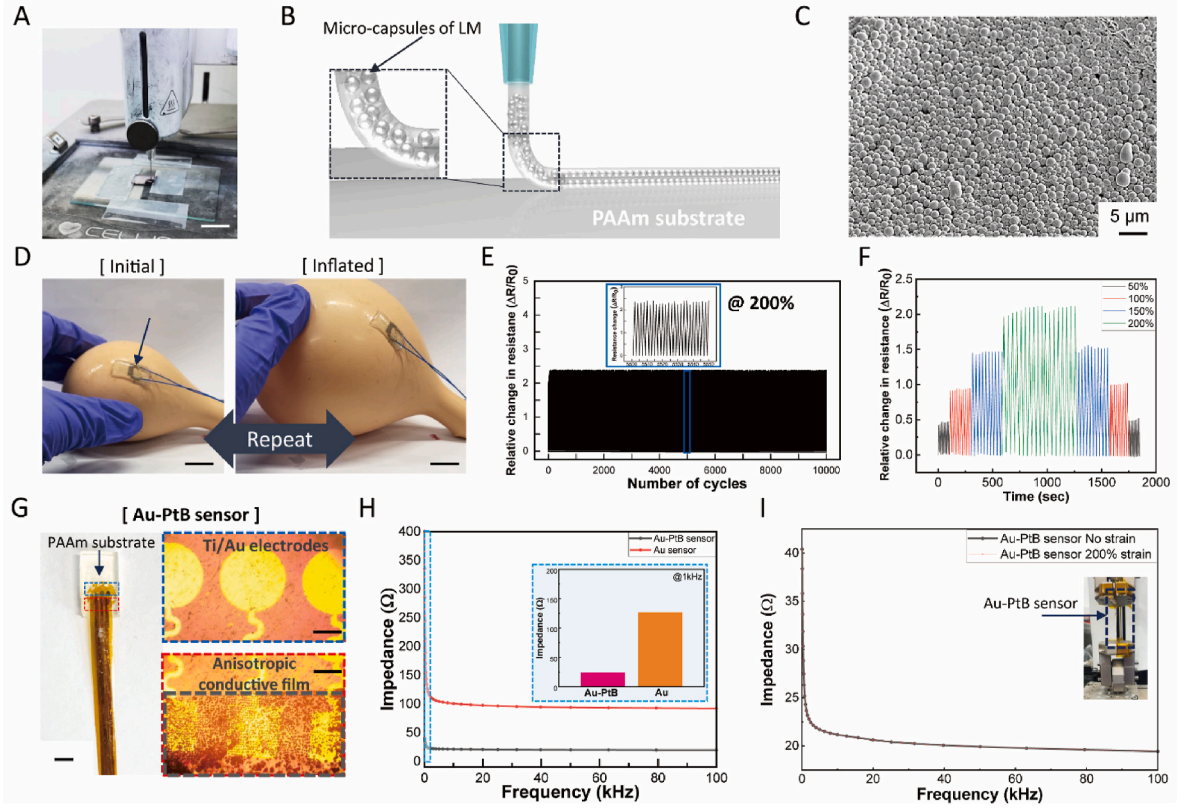

Fig. 2. (A) The photograph of meniscus-guided coating of EGaIn* (EGaIn liquid metal particle) on a PAAm substrate. Scale bar, 10 mm; (B) Schematic illustration of printed EGaIn* on PAAm substrate; (C) SEM images of printed EGaIn* on PAAm substrate; (D) Photograph of mimicking micturition using artificial bladder. Scale bar, 5 mm; (E) The plot of relative resistance change of the strain sensor under repeated 10,000 cycles at 200% strain; (F) Plot of relative resistance change under various strains; (G) The photograph (Scale bar, 5 mm) and optical microscopy images of the EMG sensor and anisotropic conductive film integrated on top (Scale bar, 100 μm); (H) Plot of impedance versus frequency of Au EMG sensor with and without Platinum black coating; (I) Plot of impedance versus frequency of EMG sensor before and after 200% strain.

diameter of 3 mm, and 3.5 mm, respectively; see Fig. S9), which was previously shown to have higher resistance to strain and fatigue (Yang et al., 2022). Fig. S9 shows higher resistance of the FWI to interfacial fatigue compared to conventional circular islets. Fig. 2I shows the impedance of the EMG sensor on FWI at zero and 200% strain, showing that impedance measurement is unaffected by strain. Fig. S10 shows the impedance before and after 10,000 cycles of applying 200% strain, which demonstrates long term durability and reliability of the EMG sensor under repeated strain.

To investigate biocompatibility of the USH-SI sensor, in-vitro live/dead cell viability of HEK293 cells from human was conducted as shown in Fig. 3A and Materials and Methods in Supporting information. Negative controls were performed by treating with 0.1% saponin for 10 min as shown Fig. S11 with quantified relative cell viability as shown in Fig. S12. The in-vivo cytotoxicity of the USH-SI sensor exhibited comparable in-vitro cytotoxicity to control (pristine HEK293 cells seeded 48-well plater with in Dulbecco Modified Eagle Medium (DMEM)) after 24 h.

The feasibility of the sensor under in-vivo condition was evaluated by attaching the USH-SI sensor on the bladder surface of urethane anesthetized Sprague-Dawley rats (SD rat). Experimental protocol for evaluation is detailed in Materials and Methods in Supporting information and in Fig. S13. Saline was injected and withdrawn repeatedly (Δ 0.3 ml within 1 s) though catheter connected to the bladder to

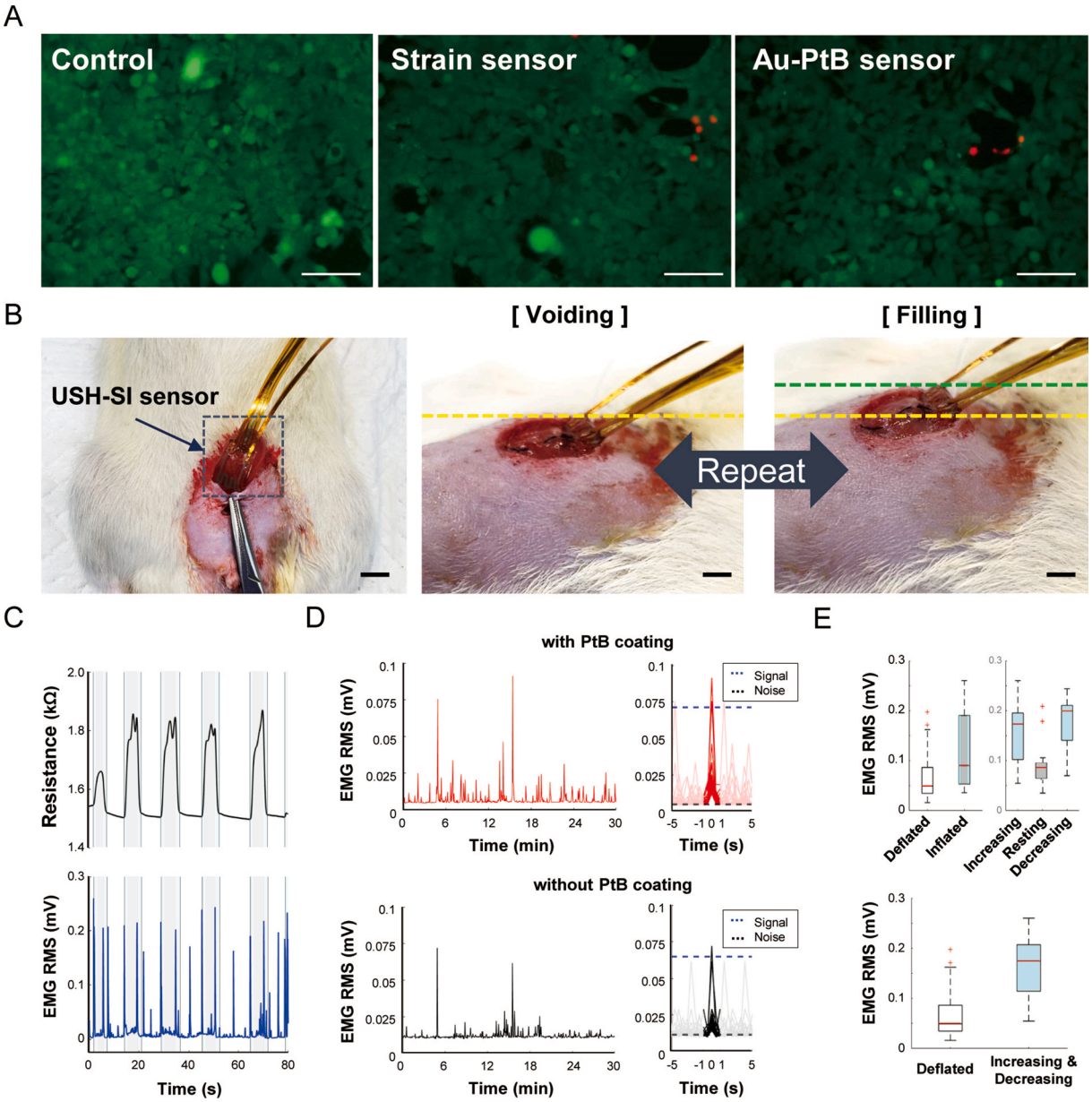

Fig. 3. (A) In-vitro cytotoxicity of a USH-SI sensor based on LIVE/DEAD cell assay after 24 h in a control media (HEK293 cells) and in a USH-SI sensor-incubated media. Live cells are shown in green and dead cells are shown in red. Scale bar, 200 μm; (B) The photographs of in-vivo protocol using rat model during repeated voiding and filling: Yellow dash line indicates initial state and Green dash line indicates filling state of bladder. Scale bar, 10 mm; (C) The plot of strain sensor resistance (top) and EMG RMS (bottom) during repeated injection and withdrawal of fluid into and out of the bladder to artificially induce bladder volume change; (D) Plot of EMG RMS from EMG sensor with (top, red) and without (bottom, black) Platinum black (PtB) coating. Left plots show simultaneously measured EMG RMS and right plots show overlapped EMG RMS. The right plots also show signal level and noise level of EMG RMS.(E) The box plot analysis of EMG RMS at different bladder states. Top left shows box plot by bladder volume, top right shows box plot at different transition states, bottom shows box plot comparing deflated state and bladder volume transitioning states.

artificially induce bladder volume change (Fig. 3B). Fig. 3C top shows the acquired strain sensor resistance during repeated injection and withdrawal. Injection increased resistance of the strain sensor, which indicates stretching of the sensor due to the increased bladder volume. Vice versa was true for withdrawing.

Fig. 3D shows EMG RMS signal of the sensor with and without PtB, tested on the same bladder. Using the ratio of the average RMS signal and RMS noise, SNR was calculated (SNR(dB) = 10 log ($Power_{Signal}$/$Power_{Noise}$) = 20 log ($Amplitude_{Signal(RMS)}$/$Amplitude_{Noise(RMS)}$). PtB coated EMG sensor shows better SNR of 22.84 dB compared to that of without PtB coating, which had SNR of 14.42 dB. This result indicates that PtB coating is feasible for increasing the signal to noise of the EMG sensor under in-vivo condition.

Fig. 3C bottom is the EMG RMS, corresponding to the same time scale as Fig. 3C top. Fig. 3E shows box plot analysis of EMG RMS at different states, as indicated in the plot. Only the EMG RMS values exceeding 2 times the RMS average (2 × 0.0115 mV = 0.0231 mV) were analyzed for the box plot. Comparing between the deflated and inflated states (top left), the inflated state showed an average RMS 1.82 times higher than that of the deflated state. We further divided the states as 1) volume increasing state under saline injection (cyan), 2) volume decreasing state under saline withdrawal (cyan), and 3) resting state between saline injection and withdrawal (gray) (top right). The resting state shows lower average RMS, whereas the other two states showed significantly higher average RMS (greater by a factor of 3.35). Comparison of the EMG RMS at deflated state and in the transitioning state (during volume

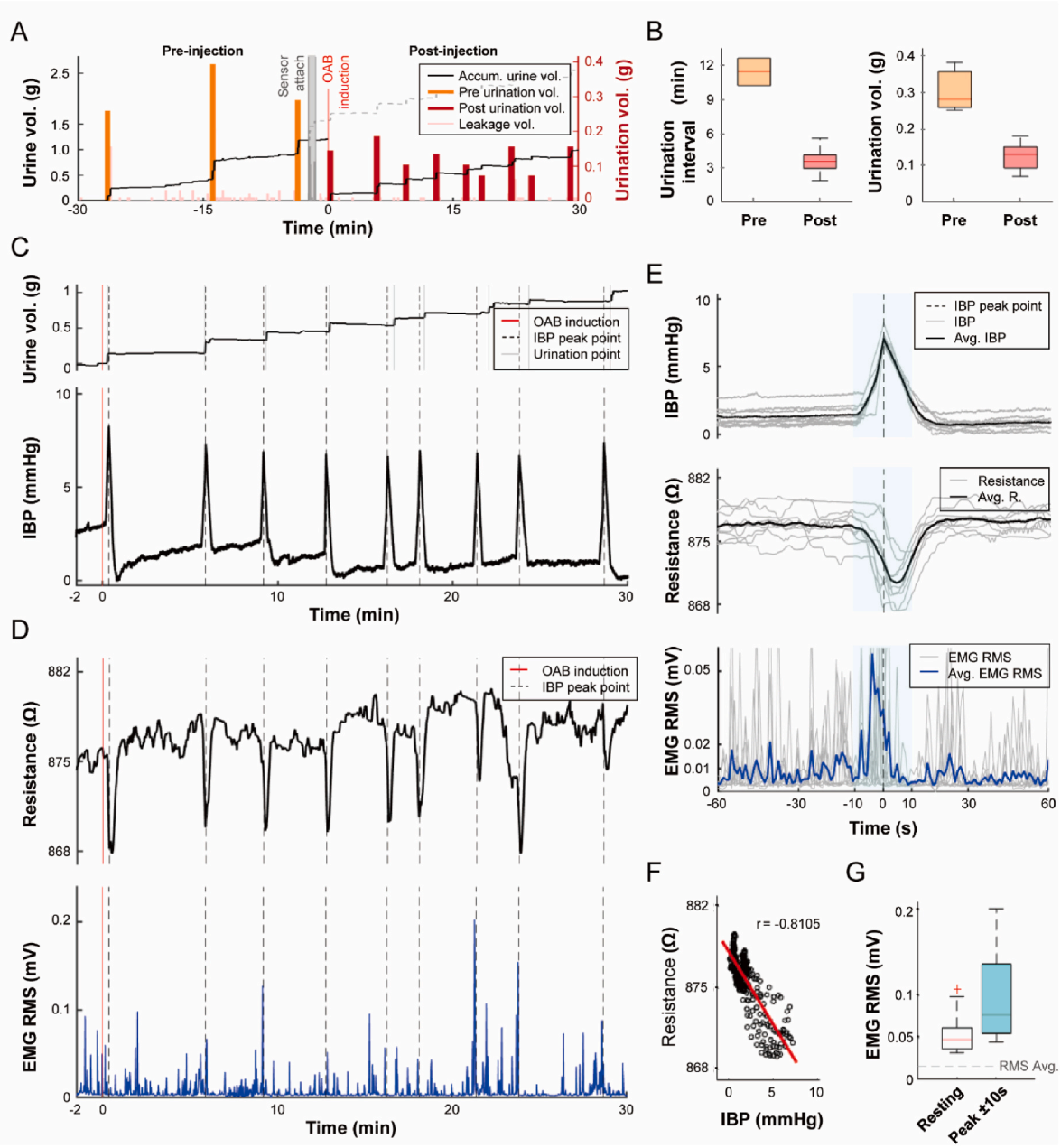

Fig. 4. (A) Plot of collected urine volume before (orange bars) and after (red bars) inducing overactive bladder (OAB). The black lines represent accumulated urine volume; (B) Box plot comparing urination interval and urination volume before and after OAB induction; (C) Plot accumulated urine volume and intra-bladder pressure (IBP); (D) Plot of strain sensor resistance and EMG RMS; (E) The plot of overlapped IBP, strain sensor resistance, and EMG RMS near the IBP peaks. Darker lines represent the averages; (F) Plot of correlation coefficient analysis between IBP and strain sensor resistance; (G) Box plot analysis of EMG RMS at rest and near the IBP peaks.

increasing and decreasing) also yielded a significant difference in the signal, as seen in Fig. 3E bottom. In-vitro aging testing was conducted as shown in Fig. S14 and in Materials and Methods in Supporting information. After one month in an in-vitro environment, the sensitivity of the strain sensor and the impedance of the EMG sensor did not undergo a significant change.

After confirming in-vivo feasibility of USH-SI sensor, we performed another in-vivo study to further validate USH-SI sensor's capability of detecting abnormal urination patterns using the OAB induced rat model. The micturition reflex control and OAB induction process by intra bladder injection is shown in Materials and Methods in Supporting information. Fig. 4 shows the highlights of the continuous monitoring of the bladder condition before and after OAB induction (red vertical line). The orange and red bars in Fig. 4A indicate collected urine volume at each point of urination, under normal and OAB induced state, respectively (the black lines indicate accumulated urine volume). Before OAB induction, urination pattern shows normal micturition reflex; while after OAB induction, urination interval and volume both decreased, indicating that OAB was successfully induced. Fig. 4B summarizes the urination activity before and after OAB induction (urination interval: 11.41 min → 3.51 min, urination volume: 0.292 g → 0.144 g). Fig. 4C and D shows the change in the urine volume and IBP due to urination, and the corresponding change in the strain sensor resistance and EMG RMS signal after OAB induction, respectively. Near the IBP peaks (dotted vertical lines), resistance and EMG RMS visually show a difference in the signal. During micturition reflex the bladder squeezes to contract itself, which manifests as abrupt increase and recovery (i.e. peak generation) in the IBP (Fig. 4C bottom). Likewise, it is apparent that the strain sensor resistance abruptly decreases and recovers, resulting downward peak generation when IBP peaks appear (Fig. 4D top). EMG RMS shows intermediate high activation and those activation points are prominently located near IBP peaks (Fig. 4D bottom). Fig. 4E are the overlap of the IBP, strain sensor resistance, and EMG RMS near IBP peaks (thus an overlap of the urination points). The response time of the proposed sensor is determined to be about 1s by measuring the difference between the IBP and the resistance change inflection points as shown in Fig. S15. The average of the strain sensor resistance and EMG RMS clearly show an increase in signal near the IBP peaks, indicating that the sensor signals can be used to monitor urination points and thus the status of OAB.

Further numerical analysis was conducted to evaluate the correlation between the sensor data and the bladder state. Fig. 4F show correlation coefficient of −0.8105 between IBP and the strain sensor resistance. Fig. 4G shows box plot of EMG RMS at IBP peaks (analyzed at the peak ±10s) and at rest (at low IBP values). Here only the EMG RMS values exceeding two times the RMS average (2×0.0157 mV = 0.0314 mV) was considered. Resting state had an average EMG RMS of 0.0471 mV; however, near the peaks, the average EMG RMS was 0.0754 mV, which was 1.81 times higher than that of the resting state. Also, standard deviation of each state show that near the IBP peaks, higher EMG RMS values were attained. These results together confirm that USH-SI sensor can probe the activity of an OAB induced bladder by detecting the urination points.

But the results from Fig. 4D show peaking of EMG activity were also intermittently observed at regions other than the urination point, making it difficult to differentiate the urination from normal states based on only peak analysis of RMS EMG. However, peak of the resistance change measured by the strain sensor was clearly distinguishable near urination, as shown in Fig. 4F. Therefore, for precise analysis of the micturition point, simultaneous use of both EMG and strain sensor is important for mutual validation and redundant analysis purpose. Nonetheless, EMG sensor will be more useful for monitoring abnormal pattern of neuropathic symptoms (Adel et al., 2013) and strain sensor for myopathic symptoms.

To further analyze the potential of our sensor for OAB monitoring, we have surgically inserted the USH-SI sensor into an anesthetized pig via surgical-robot assisted laparoscopic surgery (K-FLEX2 flexible endoscopic surgical robot by ROEN Surgical was used for this study). Fig. 5A, 5B, and S16 are the schematic depiction and picture of the robotic arm being inserted through an incision made near the pig's umbilical area. The USH-SI sensor was inserted using another port with a diameter of 12 mm. The sensor's dimensions were 10 mm by 15 mm in area, which was a proper device size to easily fit through this port. We note that with the previous bladder activity devices that needs to be large to cover or surround the entire bladder (Hwang et al., 2014; Maeso et al., 2010), laparoscopic insertion is projected to be very difficult. For the attachment of sensor on bladder in human patients in the future, robot-assisted laparoscopic surgery is potentially beneficial since it opens up the possibility to place the sensor inside the patient using a minimal single incision, causing less complications and side effects to the patient after surgery due to minimal blood loss and dissection (Maeso et al., 2010). The external wiring on the sensor was made long enough to electrical connect sensor to a measurement equipment located outside. The external wiring was passed through the laparoscopic trocar and no gas leakage was observed. An intra-abdominal pressure was maintained at 15 mmHg. After insertion of the sensor, the robotic arm was remotely manipulated to attach the sensor on the surface of the bladder, as depicted in Fig. 5C. The robotic arm had 5 degrees of freedom (pitch/yaw/rotation/translation/grasping), thus enabling complex movements. With gentle application of pressure, the USH-SI sensor firmly attached onto the bladder tissue. Fig. 5D are the pictures of the bladder-attached sensor under voiding and filling, showing stable attachment. Fig. 5E and F are strain sensor resistance and EMG RMS during artificial voiding and filling of pig bladder. Fig. 5E shows increase in strain sensor resistance under fluid injection (filling) and decrease under withdrawal (voiding). Fig. 5F is the strain sensor resistance and EMG RMS under withdrawal. Higher values of EMG RMS are seen during sudden bladder volume drop (i.e. sudden decrease in impedance), similar to the results observed in Fig. 3C. These results show that the USH-SI sensor can probe the bladder activity on both small and large animal subjects (rat and the pig), showing its operation regardless of bladder size, thus opening up the possibility of using USH-SI sensor on patients in the future for OAB monitoring.

3. Conclusion

In this work, an implantable bladder activity sensor (namely USH-SI sensor) was developed for continuous monitoring of OAB. As stated in the Introduction, the full electromechanical characterization of bladder activity is required to elucidate the mechanisms of OAB symptoms. Contrary to previously reported sensors, our USH-SI sensor is ultra-soft (with a low modulus of 1 kPa) and adheres well onto bladder tissue. These properties enable stable device operation without obstructing the natural movement of the bladder. Furthermore, these properties enable implantation via laparoscopic surgery, which would be beneficial to the patient due to minimal tissue dissection and fast recovery time. The strain sensor was made with printed liquid metal particle-based thin-film lines, which due to their high stretchability and mechanical durability, enables reliable strain measurement under repeated cycles of high strains. EMG sensor was placed on structurally-engineered rigid PI islets that increased fatigue resistance under high strains. In OAB induced rat model and aestheticized pig, the strain and EMG sensor clearly produced higher signals during bladder movement, thus confirming their feasibility for continuous OAB monitoring. For future work, bio-adhesive will be synthesized with oxidative polymer or hydrogel materials to improve underwater adhesion. In addition, packaging technology for long-term in-vivo reliability and new wiring technology to prevent wrinkling during continuous monitoring of freely moving animals will be developed. Finally, high resolution and multi-array sensors will be developed for spatial-temporal analysis of bladder activity. These advances would further legitimize the sensor as a continuous monitoring device, inching it closer towards clinical applications. In addition, a fully implantable

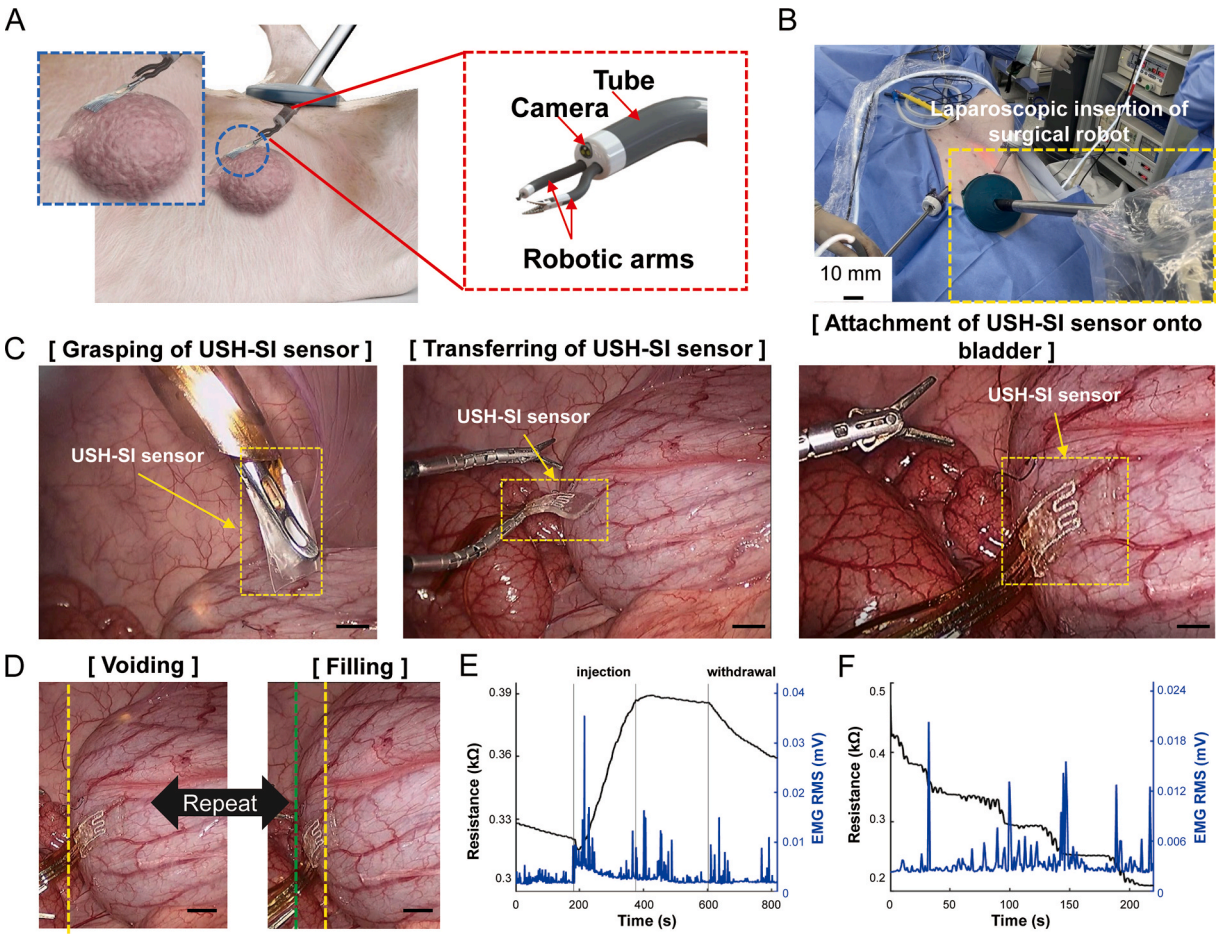

Fig. 5. (A) and (B) Schematic illustration (A) and photograph (B) of robot-assisted laparoscopic surgery for implantation of USH-SI sensor onto a pig's bladder; (C) Photographs showing the attachment process of USH-SI sensor onto the bladder using robotic arm manipulation. Scale bar, 10 mm; (D) Photograph of repeated voiding and filling. Yellow dash line indicates initial state and Green dash line indicates filling state of bladder. Scale bar, 10 mm; (E) The plot of strain sensor resistance and EMG RMS under injection and withdrawal of fluid into and out of the pig bladder; (F) The plot of strain sensor resistance and EMG RMS during withdrawal.

feedback system that includes both a neurostimulator and sensor is underway for both diagnosis and effective treatment of OAB. These are exciting prospects, not only for the treatment of OAB but also other neurological disorders. The sensor reported in this work is the first critical step towards this ultimate goal.

CRediT authorship contribution statement

Byungkook Oh: Conceptualization, Data curation, Formal analysis, Investigation, Methodology, Validation, Visualization, Writing – original draft. **Young-Soo Lim:** Data curation, Formal analysis, Investigation, Methodology, Validation, Visualization, Writing – original draft. **Kun Woo Ko:** Data curation, Methodology. **Hyeonyeob Seo:** Visualization, Methodology. **Dong Jun Kim:** Formal analysis, Investigation, Methodology. **Dukyoo Kong:** Formal analysis, Methodology, Resources, Software. **Jae Min You:** Formal analysis, Methodology, Resources, Software. **Hansoul Kim:** Formal analysis, Methodology, Resources, Software. **Taek-Soo Kim:** Supervision. **Seongjun Park:** Supervision. **Dong-Soo Kwon:** Resources, Software, Supervision. **Joon Chae Na:** Resources, Supervision. **Woong Kyu Han:** Resources, Supervision. **Sung-Min Park:** Conceptualization, Supervision, Writing – review & editing, Funding acquisition, Project administration. **Steve Park:** Conceptualization, Supervision, Writing – review & editing, Funding acquisition, Project administration, All authors discussed the results and contributed to the final manuscript.

Declaration of competing interest

The authors declare that they have no known competing financial interests or personal relationships that could have appeared to influence the work reported in this paper.

Data availability

No data was used for the research described in the article.

Acknowledgements

We thank Jeongdo Ahn for surgical robot master design, Joonhwan Kim and Kwang-Soo Baek for assisting in robot-assisted laparoscopic surgery. This research was supported by the Pioneer Research Center Program through the National Research Foundation of Korea funded by the Ministry of Science, ICT & Future Planning (2022M3C1A3081294) and by the National Research Foundation of Korea (NRF-2021M3H4A1A03049049).

Appendix A. Supplementary data

Supplementary data to this article can be found online at https://doi.org/10.1016/j.bios.2023.115060.

References

Abbott, J., Ye, T., Krenek, K., Gertner, R.S., Ban, S., Kim, Y., Qin, L., Wu, W., Park, H., Ham, D., 2020. A nanoelectrode array for obtaining intracellular recordings from thousands of connected neurons. Nat. Biomed. Eng. 4, 232–241. https://doi.org/10.1038/s41551-019-0455-7.

Adel, T., Stashuk, D., Adel, T., Stashuk, D., 2013. Clinical Quantitative Electromyography, Electrodiagnosis in New Frontiers of Clinical Research. IntechOpen. https://doi.org/10.5772/56033.

Arab Hassani, F., Jin, H., Yokota, T., Someya, T., Thakor, N.V., 2020. Soft sensors for a sensing-actuation system with high bladder voiding efficiency. Sci. Adv. 6 https://doi.org/10.1126/sciadv.aba0412 eaba0412.

Banakhar, M.A., Al-Shaiji, T., Hassouna, M., 2012. Sacral neuromodulation and refractory overactive bladder: an emerging tool for an old problem. Ther. Adv. Urol. 4, 179–185. https://doi.org/10.1177/1756287212445179.

Bovone, G., Dudaryeva, O.Y., Marco-Dufort, B., Tibbitt, M.W., 2021. Engineering hydrogel adhesion for biomedical applications via chemical design of the junction. ACS Biomater. Sci. Eng. 7, 4048–4076. https://doi.org/10.1021/acsbiomaterials.0c01677.

Chen, Y., Kim, Y.-S., Tillman, B.W., Yeo, W.-H., Chun, Y., 2018. Advances in materials for recent low-profile implantable bioelectronics. Materials 11, 522. https://doi.org/10.3390/ma11040522.

Chiew, C., Morris, J., Malakooti, M, M.H., 2021. Functional liquid metal nanoparticles: synthesis and applications. Mater. Adv. 2, 7799–7819. https://doi.org/10.1039/D1MA00789K.

Chitrakar, C., Hedrick, E., Adegoke, L., Ecker, M., 2022. Flexible and stretchable bioelectronics. Materials 15, 1664. https://doi.org/10.3390/ma15051664.

Fowler, C.J., Griffiths, D., de Groat, W.C., 2008. The neural control of micturition. Nat. Rev. Neurosci. 9, 453–466. https://doi.org/10.1038/nrn2401.

Herbison, G.P., Arnold, E.P., 2009. Sacral neuromodulation with implanted devices for urinary storage and voiding dysfunction in adults. Cochrane Database Syst. Rev. https://doi.org/10.1002/14651858.CD004202.pub2.

Hwang, H., Kong, M., Kim, K., Park, D., Lee, S., Park, S., Song, H.-J., Jeong, U., 2021. Stretchable anisotropic conductive film (S-ACF) for electrical interfacing in high-resolution stretchable circuits. Sci. Adv. 7, eabh0171 https://doi.org/10.1126/sciadv.abh0171.

Hwang, M., Chung, H., Kwon, D.-S., 2014. A portable endoscopic tool handler (PETH) with its ex-vivo ESD trials. In: 2014 11th International Conference on Ubiquitous Robots and Ambient Intelligence (URAI). Presented at the 2014 11th International Conference on Ubiquitous Robots and Ambient Intelligence. URAI), pp. 85–87. https://doi.org/10.1109/URAI.2014.7057401.

Jang, T.-M., Lee, J.H., Zhou, H., Joo, J., Lim, B.H., Cheng, H., Kim, S.H., Kang, I.-S., Lee, K.-S., Park, E., Hwang, S.-W., 2020. Expandable and implantable bioelectronic complex for analyzing and regulating real-time activity of the urinary bladder. Sci. Adv. 6, eabc9675 https://doi.org/10.1126/sciadv.abc9675.

Ju, C., Park, E., Ye, E., Kim, Y.-G., Kim, T., Kang, M., Shon, Y.-M., Lee, K.-S., Park, S.-M., 2022. Fabrication of a flexible three-dimensional hybrid directional lead for deep brain stimulation and control of micturition reflex in rats. IEEE Access 10, 86833–86843. https://doi.org/10.1109/ACCESS.2022.3198980.

Kim, J., Ghaffari, R., Kim, D.-H., 2017. The quest for miniaturized soft bioelectronic devices. Nat. Biomed. Eng. 1, 1–4. https://doi.org/10.1038/s41551-017-0049.

Kim, J.-H., Kim, S., So, J.-H., Kim, K., Koo, H.-J., 2018. Cytotoxicity of gallium–indium liquid metal in an aqueous environment. ACS Appl. Mater. Interfaces 10, 17448–17454. https://doi.org/10.1021/acsami.8b02320.

Lacour, S.P., Courtine, G., Guck, J., 2016. Materials and technologies for soft implantable neuroprostheses. Nat. Rev. Mater. 1, 1–14. https://doi.org/10.1038/natrevmats.2016.63.

Lai, H.H., Rawal, A., Shen, B., Vetter, J., 2016. The relationship between anxiety and overactive bladder or urinary incontinence symptoms in the clinical population. Urology 98, 50–57. https://doi.org/10.1016/j.urology.2016.07.013.

Lee, C.-J., Wu, H., Hu, Y., Young, M., Wang, H., Lynch, D., Xu, F., Cong, H., Cheng, G., 2018. Ionic conductivity of polyelectrolyte hydrogels. ACS Appl. Mater. Interfaces 10, 5845–5852. https://doi.org/10.1021/acsami.7b15934.

Lee, G.-H., Lee, Y.R., Kim, Hanul, Kwon, D.A., Kim, Hyeonji, Yang, C., Choi, S.Q., Park, Seongjun, Jeong, J.-W., Park, Steve, 2022. Rapid meniscus-guided printing of stable semi-solid-state liquid metal microgranular-particle for soft electronics. Nat. Commun. 13, 2643. https://doi.org/10.1038/s41467-022-30427-z.

Lee, U.J., Ward, J.B., Feinstein, L., Matlaga, B.R., Martinez-Miller, E., Bavendam, T., Kirkali, Z., Kobashi, K.C., 2021. National trends in neuromodulation for urinary incontinence among insured adult women and men, 2004-2013: the urologic diseases in America project. Urol., Women's Health Urol. 150, 86–91. https://doi.org/10.1016/j.urology.2020.11.043.

Li, C., Guan, G., Zhang, F., Song, S., Wang, R.K., Huang, Z., Nabi, G., 2014. Quantitative elasticity measurement of urinary bladder wall using laser-induced surface acoustic waves. Biomed. Opt Express 5, 4313–4328. https://doi.org/10.1364/BOE.5.004313.

Lo, M.-C., Widge, A.S., 2017. Closed-loop neuromodulation systems: next-generation treatments for psychiatric illness. Int. Rev. Psychiatr. 29, 191–204. https://doi.org/10.1080/09540261.2017.1282438.

Maeso, S., Reza, M., Mayol, J.A., Blasco, J.A., Guerra, M., Andradas, E., Plana, M.N., 2010. Efficacy of the Da Vinci surgical system in abdominal surgery compared with that of laparoscopy: a systematic review and meta-analysis. Ann. Surg. 252, 254–262. https://doi.org/10.1097/SLA.0b013e3181e6239e.

Meng, E., Lin, W.-Y., Lee, W.-C., Chuang, Y.-C., 2012. Pathophysiology of overactive bladder. Low. Urin. Tract. Symptoms 4, 48–55. https://doi.org/10.1111/j.1757-5672.2011.00122.x.

Millard, R.J., Halaska, M., 2006. Efficacy of solifenacin in patients with severe symptoms of overactive bladder: a pooled analysis. Curr. Med. Res. Opin. 22, 41–48. https://doi.org/10.1185/030079905X74907.

Mirza, K.B., Golden, C.T., Nikolic, K., Toumazou, C., 2019. Closed-loop implantable therapeutic neuromodulation systems based on neurochemical monitoring. Front. Neurosci. 13.

Nagai, K., Homma, Y., Ideno, Y., Hayashi, K., 2021. Prevalence and factors associated with overactive bladder and stress urinary incontinence in the Japan Nurses' Health Study. Menopause 29, 129–136. https://doi.org/10.1097/GME.0000000000001893.

Pei, X., Wang, J., Cong, Y., Fu, J., 2021. Recent progress in polymer hydrogel bioadhesives. J. Polym. Sci. 59, 1312–1337. https://doi.org/10.1002/pol.20210249.

Redmond, E.J., 'Kelly Therese, O., Flood, H.D., 2019. The effect of bladder filling rate on the voiding behavior of patients with overactive bladder. J. Urol. 202, 326–332. https://doi.org/10.1097/JU.0000000000000199.

Roche, E.T., 2019. Implanted device enables responsive bladder control. Nature 565, 298–300. https://doi.org/10.1038/d41586-018-07811-1.

Scarneciu, I., Lupu, S., Bratu, O.G., Teodorescu, A., Maxim, L.S., Brinza, A., Laculiceanu, A.G., Rotaru, R.M., Lupu, A.-M., Scarneciu, C.C., 2021. Overactive bladder: a review and update. Exp. Ther. Med. 22, 1444. https://doi.org/10.3892/etm.2021.10879.

Seiffert, S., Oppermann, W., 2007. Amine-functionalized polyacrylamide for labeling and crosslinking purposes. Macromol. Chem. Phys. 208, 1744–1752. https://doi.org/10.1002/macp.200700151.

Seo, J.-W., Kim, H., Kim, K., Choi, S.Q., Lee, H.J., 2018. Calcium-modified silk as a biocompatible and strong adhesive for epidermal electronics. Adv. Funct. Mater. 28, 1800802 https://doi.org/10.1002/adfm.201800802.

Shimoni, Z., Fruger, E., Froom, P., 2015. Measurement of post-void residual bladder volumes in hospitalized older adults. Am. J. Med. 128, 77–81. https://doi.org/10.1016/j.amjmed.2014.08.018.

Someya, T., Bao, Z., Malliaras, G.G., 2016. The rise of plastic bioelectronics. Nature 540, 379–385. https://doi.org/10.1038/nature21004.

Steers, W.D., 2002. Pathophysiology of overactive bladder and urge urinary incontinence. Rev. Urol. 4 (4), S7–S18.

Wellman, S.M., Eles, J.R., Ludwig, K.A., Seymour, J.P., Michelson, N.J., McFadden, W.E., Vazquez, A.L., Kozai, T.D.Y., 2018. A materials roadmap to functional neural interface design. Adv. Funct. Mater. 28, 1701269 https://doi.org/10.1002/adfm.201701269.

Yang, J.C., Lee, S., Ma, B.S., Kim, J., Song, M., Kim, S.Y., Kim, D.W., Kim, T.-S., Park, S., 2022. Geometrically engineered rigid island array for stretchable electronics capable of withstanding various deformation modes. Sci. Adv. 8, eabn3863. https://doi.org/10.1126/sciadv.abn3863.

Yuk, H., Lu, B., Zhao, X., 2019. Hydrogel bioelectronics. Chem. Soc. Rev. 48, 1642–1667. https://doi.org/10.1039/C8CS00595H.

Yuk, H., Wu, J., Zhao, X., 2022. Hydrogel interfaces for merging humans and machines. Nat. Rev. Mater. 7, 935–952. https://doi.org/10.1038/s41578-022-00483-4.

Zhang, H., Cheng, Y., Hou, X., Yang, B., Guo, F., 2018. Ionic effects on the mechanical and swelling properties of a poly(acrylic acid/acrylamide) double crosslinking hydrogel. New J. Chem. 42, 9151–9158. https://doi.org/10.1039/C8NJ00920A.